Correlation Between Microstructure, Magnetic Properties And Mechanical Behavior of The Permimphy Alloy After High-Pressure Torsion

Oussama Dabou[a,b*], Thierry Baudin[a], François Brisset[a], Thierry Waeckerlé[c], Yanick Ateba Betanda[c], Yi Huang[d,e], Anne-Laure Helbert[a], Djamel Bradai[b] and Terence G. Langdon[e]

[(a)] Université Paris-Saclay, CNRS, Institut de chimie moléculaire et des matériaux d'Orsay, 91405 Orsay, France.
[(b)] Physique des Matériaux, Faculté de Physique, Université des Sciences et de la Technologie Houari Boumediene, Bab Ezzouar, BP32, El Alia, Alger, Algérie.
[(c)] Research Center, Aperam Alloys, rue P. Chevenard, Imphy 58160, France.
[(d)] Department of Design and Engineering, Faculty of Science and Technology, Bournemouth University, Poole, Dorset BH12 5BB, United Kingdom
[(e)] Materials Research Group, Department of Mechanical Engineering, University of Southampton, Southampton SO17 1BJ, UK

Abstract

This study investigates the correlation between coercivity (*H*c), grain size (*d*), and dislocation density in the Permimphy alloy (Fe-80%Ni-6%Mo). The samples used in this study were subjected to varying levels of applied strain through processing by high-pressure torsion (HPT). The microstructure and the magnetic coercivity were analyzed using a scanning electron microscope (SEM), Electron Backscatter Diffraction (EBSD) and Vibrating Sample Magnetometry (VSM). The grain size of the samples varied from 30 µm to 190 nm. This study demonstrated a strong correlation between *H*c and microhardness when d > 3 µm. The results show that the coercivity of the Permimphy alloy follows an inverse V-shape with respect to grain size. The coercivity of the samples decreased despite increasing the dislocation density and the hardness when $d < 3$ µm. This phenomenon is attributed to the ferromagnetic exchange interaction across multiple grains and leads to the alignment of magnetic moments.

Keywords: Permimphy, high-pressure torsion, microstructure, hardness, coercivity. Dislocations.

[*] Corresponding author E-mail: dabououssama@gmail.com

1. Introduction

Soft magnetic materials (SMMs) are used for transformers, motors, and sensors. This requires very low coercivity and the highest possible susceptibility (or permeability), which is equivalent to weak anisotropy and easy magnetization [1] . The SMMs are usually characterized by an intrinsic coercivity of less than 1000 A/m [2]. However, new SMMs with higher strength and ductility are needed to operate under mechanically demanding loading conditions for safety and for critical parts in transportation and energy [3]. In practice, Fe-Ni alloys have been developed and utilized in specialized applications [4]. Typically, these materials crystallize in face-centered cubic (FCC) structure (> 30% by weight) within the Fe-Ni group and are supplemented with various elements in small amounts. Presently, 80%Ni Permalloy materials showcase significant magnetic properties, such as an adjustable low coercive magnetic field strength, shallow energy losses and a high magnetic permeability achieved through certain special heat treatments [4]. The Permimphy alloy is a high-quality industrial grade material that possesses favorable magnetic properties, thereby making it an excellent candidate material for the precision cutting of intricate profiles.

In order to achieve the highest magnetic permeability state in this alloy, standardized heat treatments are undertaken at high temperature (>1000°C) under controlled atmospheres of vacuum or hydrogen [5]. The Permimphy alloy has a unique combination of high magnetic permeability, high electrical resistivity and low magnetic hysteresis that make it an effective shield against external magnetic fields to protect electronic devices. In general, the magnetic behavior of SMMs is influenced by several factors, including their chemical composition [6], electromagnetic anisotropy intrinsic features (first order anisotropy constants K1, magnetostriction constants $\lambda 100$, $\lambda 111$), microstructure characteristics such as texture or average grain size, the degree of atomic

order [7, 8], chemical segregation, precipitates, and non-magnetic phases. Overall, the magnetic properties of SMMs are influenced by a complex interplay of these and other factors and this means that optimizing these properties for a specific application often requires a careful balancing of these factors. The grain size (*d*) plays a crucial role because it influences – among other elements - the mobility of magnetic domain walls and the hysteresis phenomenon. More than grain boundaries (GBs), the microstructure characteristics, such as texture, dislocation distribution and density and stacking faults greatly influence the macroscopic magnetic behavior. The Empirical relationships between grain size and coercivity [9–12] indicates that conventional (d > few μm) polycrystalline materials exhibit a 1/*d* dependence whereas nanocrystalline materials (d<<μm) show a coercive field Hc which acts - experimentally and theoretically (Random Anisotropy Model) proportionally to d^6 . The origin of this lies in a spatial averaging magnetocrystalline anisotropy (balancing locally the exchange interaction between neighboring nanocrystals inside the same magnetic wall mechanism called "random anisotropy"). This mechanism becomes dominant typically when *d* is smaller than the ferromagnetic exchange length *L* [13]. Typical values of *L* are 5-10 nm for Co-based alloys and 20-40 nm for Fe-based alloys where the exchange length of the Permimphy™ is ~1-3 μm [14]. The latter appears, through the high L magnitude, the best candidate to achieve microstructure width d < L. This means that Permimphy™ is a suitable candidate for examining the transition from rising to declining coercivity, *Hc* with grain size. This could lead to the development of a novel polycrystalline magnetic materials with high mechanical strength and soft magnetic properties.

Several procedures are now available for producing sub-micrometer and nanocrystalline materials and these are based on the application of severe plastic deformation (SPD) capable of achieving large quantities of fully-dense small scale microstructures. Among these various SPD

techniques, the major procedures are High-Pressure Torsion (HPT) [15], Accumulative Roll-Bounding (ARB) [16] and Equal-Channel Angular Pressing (ECAP) [17]. Generally, HPT processing produces a greater grain refinement than the other SPD procedures [18, 19] and, in addition, HPT leads to a higher fraction of high-angle grain boundaries [20, 21].

Motivated by this background, the present research was undertaken to identify the relationships between the coercivity, grain size, grain boundary misorientations and the dislocation density. The overall objective was to explore the point at which the coercivity of the Permimphy alloy changes from increasing to decreasing with grain size, where this is indicative of the magnetic exchange length of the alloy. Thus, it is anticipated that this research will pave the way for developing SMMs with improved mechanical properties using cost-effective techniques and protocols.

2. Experimental materials and procedures

The Permimphy™ alloy (Ni15Fe5Mo in wt. %) was provided by the APERAM Alloys Imphy Company, France. The samples were in the form of rolled sheets subjected to annealing under an H_2 controlled atmosphere to fully recrystallize the alloy. For HPT processing, disks with diameters of 10 mm were cut from the initial material using wire electrical discharge machining. The thickness of the samples was then reduced to 0.85 mm using SiC grits. These disks were processed at ambient temperature up to 1/2, 5, 10 and 20 turns under a pressure of 6.0 GPa and a rotational speed of 1 rpm under quasi-constrained conditions where there is a small outflow of material around the periphery of the disk during the straining operation [22].

The microstructure and texture were characterized using a scanning electron microscope (SEM) FEG-SEM SUPRA 55 VP operating at 20 kV with TSL Orientation Imaging Microscopy, OIM™ software. EBSD maps were collected at the mid-radius of each disk on zones perpendicular

to the HPT rotation axis (RD-SD) plane where RD and SD denote the rotational and shear directions, respectively. The samples were mechanically polished using 800, 1200 and 2400 SiC sand disk, then electrolytic polishing was conducted at ambient temperature using an A2 Struers electrolyte at 20 V for 15 s. The grain size data were obtained using a grain tolerance angle of 5° and the minimum grain size was chosen as 2 pixels. All datum points with a confidence index (CI) lower than 0.05 were excluded from the analysis where CI quantifies the reliability of the indexed patterns.

The dislocation density was estimated using the Kernel Average Misorientation (KAM) method implemented within the OIM software. In this method, the misorientation KAM around the central point of a grain is quantified in relation to a defined set of nearest neighboring points. The dislocation density was then calculated using the following equation [23] :

$$\rho = \frac{\alpha\theta_{KAM}}{n\delta\mathbf{b}} \quad \ldots\ldots\ldots\ldots\ldots\ldots (1)$$

where *a* is a parameter that depends on the grain boundary type and it was chosen as 3 for boundaries mixed of the two types [24], **b** is the Burgers vector (0.254 nm for Fe-Ni alloys), $n = 3$ for nearest neighbors and δ is the size of the EBSD scan step.

The Vickers microhardness was measured by a SHIMADZU type HMV-2 using a load of 0.1 kg and a dwell time of 10 s for all measurements. At least 8 points of microhardness were measured at the mid-radius of all the HPT samples and averaged to report the microhardness of the sample. In addition, measurements were taken along the diameter of the disk in the radial direction in a rectilinear grid pattern. The distance between each indentation was set at 0.3 mm.

Magnetization curves were measured using a MicroSense vibrating sample magnetometer (VSM) at room temperature. Flat specimens with a diameter of 5 mm and a thickness of about 0.5

mm were machined from the HPT-processed disks. The maximum applied magnetic field was 2.5 T.

3. Results and discussion

3.1 Microstructure of the as-received material

The RD-ND inverse pole figures (IPFs) and Image Quality (IQ) maps of the as-received sample are shown in Figure 1(a) and Figure 1(b). The microstructure was composed of equiaxed grains with a mean grain size of ~30 µm. In Figure 1(b), low-angle grain boundaries (LAGBs) with misorientation angles between 2° and 15° and high-angle grain boundaries (HAGBs) are colored red and blue, respectively. The histogram of misorientation angles (Figure 1(c)) reveals a large fraction of HAGBs and a strong maximum near 60° associated with the presence of Σ3 boundaries (60° <111>) indicated in yellow in Fig. 1c. These have been widely reported after conventional thermo-mechanical processing (TMP) of FCC materials with low to medium stacking fault energy [25].

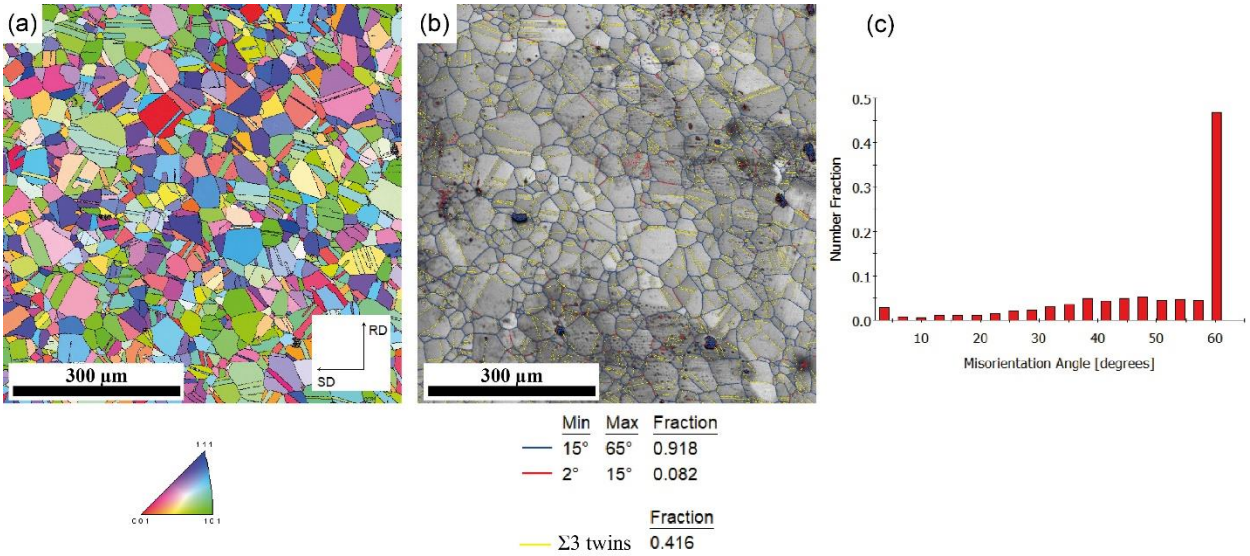

Figure 1: (a)TD- IPF-map, (b) IQ-map with grain boundaries, (c) misorientation angle distribution of the as-received material.

3.2 Microstructure of Permimphy^{TM} alloy after HPT

Figure 2 compiles the Normal Direction (ND) IPF micrographs showing the microstructures of the HPT-processed Permimphy^{TM} alloy at room temperature. A significant orientation spread within the individual grains due to the development of a substructure is observed in the IPF maps after 1/2 turn (Figure 2(a)). Moreover, the IPF maps after 1/2 HPT turn exhibit a bimodal grain size distribution with a large fraction of coarse grains mixed with several regions containing relatively fine grains

Figure 2 comprises ND IPF micrographs illustrating the microstructures of the HPT-processed Permimphy alloy at room temperature. The IPF maps after 1/2 turn (Figure 2(a)) reveal a notable spread in orientation within individual grains due to substructure development. Additionally, these maps display a bimodal grain size distribution after 1/2 HPT turn, featuring both coarse and relatively fine grains in different regions. It was proposed that grain subdivision serves as the prevalent mechanism in generating ultrafine microstructures through extremely severe deformation (using various SPD techniques) [26]. This formation process is often termed grain fragmentation, in-situ recrystallization and continuous dynamic recrystallization [26]. As the applied strain increased (> 5 turns), the microstructure gradually became more uniform, showing equiaxed grains somewhat elongated in the shear direction. The restructuring of grains is due to the accumulation of LAGBs observed in the microstructure after 1/2 HPT turns which contributes to the formation of new dense walls with HAGBs. This elucidates the sharp decrease in LAGBs after 5 HPT turns, as depicted in Figure 3.

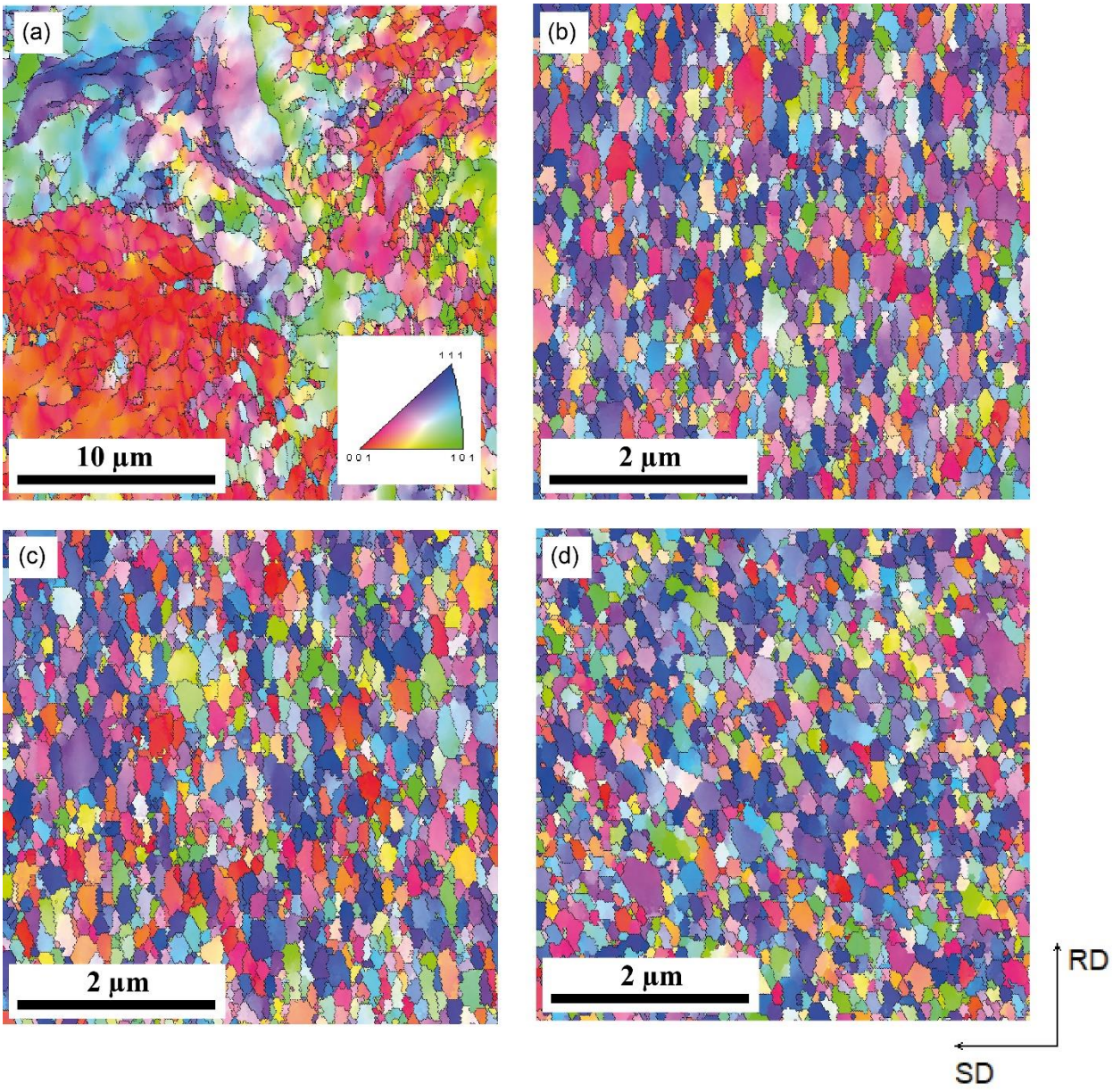

Figure 2: ND-IPF orientation imaging micrographs (EBSD maps) showing the microstructures of Permimphy^{TM} alloy after HPT deformation; (a) 1/2 turn, (b) 5 turns, (c) 10 turns and (d) 20 turns.

The evolution of the mean grain size and the HAGBs as a function of the numbers of HPT turns is shown in Figure 3. The grains underwent a strong refinement upon straining such that the mean grain size decreased from 30 µm for the as-received sample to an average of 3.5 µm after 1/2 HPT

turn, and thereafter it decreased to 205 nm after 5 turns and stabilized with a value of ~188 nm after 20 turns.

This is indicative of the success of the HPT process in achieving a sub-micrometer/nano-scale grain size distribution. The fraction of HAGBs increases rapidly after 1/2 HPT turn from 30% to 75 % after 5 HPT turns and then reaches a maximum value of 79 % after 20 HPT turns. As previously noted, this validates the aggregation of LAGBs to create high-angle boundaries within the microstructure.

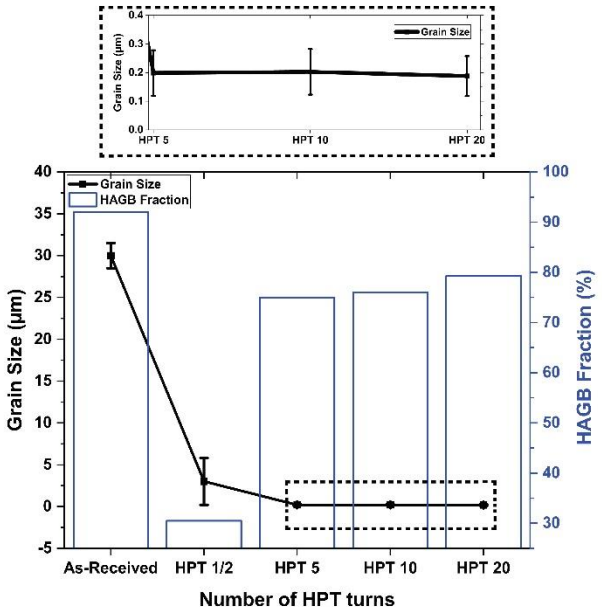

Figure 3: Evolution of the mean grain size and HAGB fraction versus the number of HPT turns

As depicted in Figure 3, subsequent deformation beyond 5 HPT turns fails to produce further grain refinement. This observation is consistent with earlier research on the impact of SPD on alloys, indicating a saturation of the grain refinement [26–32]. Previous studies have proposed various explanations for this phenomenon. A straightforward and rational suggestion involves the interplay between the grain subdivision aspect of the refinement process and other coarsening mechanisms such as recovery, grain boundary migration and triple junction motion [30].

Figure 4 shows the misorientation histograms of the the Permimphy^{TM} alloy after HPT processing. It is obvious that after 1/2 HPT turn the microstructure contains substantial amount of LAGBs. This is an indication of a substructure formation subsequent to the SPD processing. Nevertheless, with increasing HPT deformation the misorientation increases so that the LAGB fraction decreases to 20% after 20 HPT turns). The high percentage of HAGBs is an indication of the occurrence of dynamic recrystallization and grain refinement by a conventional subdivision mechanism [33]. Both phenomena lead to a progressive replacement of the LAGBs by HAGBs created by the application of the SPD processing.

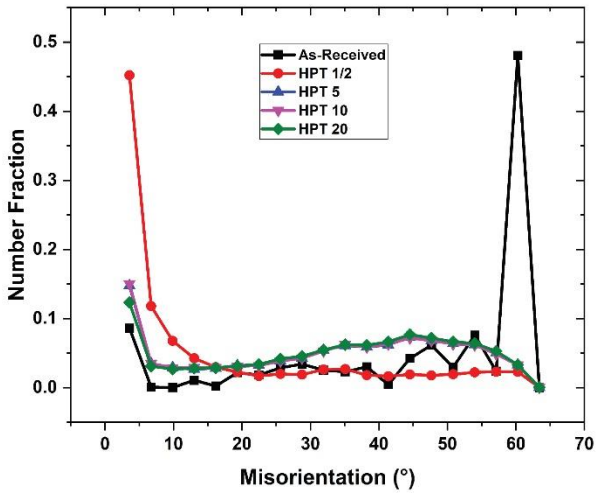

Figure 4: Evolution of the misorientation histograms after HPT processing.

As shown in Figure 5, for the as-received sample almost the entire map is represented by the blue color ascribed to weakly deformed areas. This is expected in a recrystallized material having less defects than after the annealing process. After 1/2 HPT turn, the KAM map in Figure 5(b)) exhibits more green color areas indicating a high dislocation density. These dislocations are present within the grains and confirm the formation of a substructure.

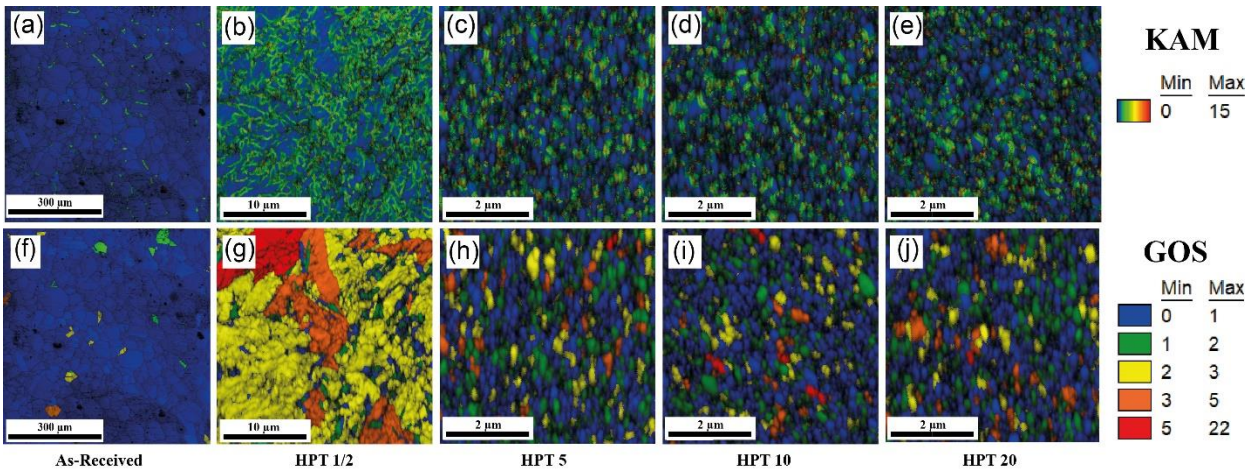

Figure 5: OIM-KAM maps and GOS maps of the as-received material and after HPT processing. (a)-(e): KAM maps of the Permimphy as received and after 1/2, 5, 10 and 20 HPT turns. (g)-(i): GOS maps of the Permimphy as received and after 1/2, 5, 10 and 20 HPT turns, respectively.

For each grain, the grain orientation spread (GOS) indicates the degree of orientation change between every pixel in the grain and the grain average orientation. Thus, a low GOS value denotes low internal misorientations which is a characteristic feature of a recrystallized state. Before HPT deformation, almost all of the grains were recrystallized owing to the initial thermo-mechanical processing of the as-received material. After ½ HPT turn, a large majority of grains (90 %) exhibited large GOS values. Further HPT deformation, as in Figure 5(h-j), leads to the generation of new grains with weaker GOS values. As already noted, these are created primarily by the two mechanisms of dynamic recrystallization during the deformation process and the accumulation of LAGBs which leads to the development of new grain boundaries.

The microhardness profile evolutions, taken from -4 mm to +4 mm from the centers of the samples, are shown in Figure 6. After 1/2 HPT turn, the microhardness is lowest in the center and highest at the edges of the disk and the difference in microhardness between the edge and the center is about 150 *Hv* (~ 55%). The imposed strain is lower in the central area of the disk leading

to a lower microhardness whereas a higher microhardness is achieved at the peripheral area receiving the highest imposed strain. However, this difference tends to become small after large numbers of turns because of the overall increase in the microhardness level, and this leads to a reasonable hardness homogeneity throughout the disk diameter with a saturation level of around 470 Hv after 5 turns. In addition, the overall microhardness across the disk increases with increasing numbers of HPT turns [34].

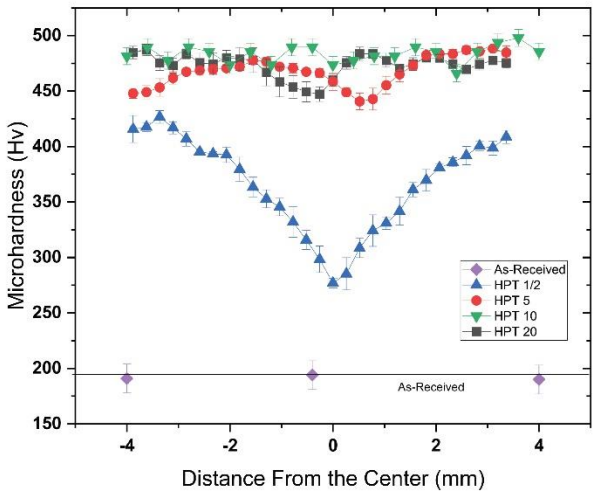

Figure 6: Microhardness distribution across the diameter of the HPT-deformed disks.

The evolution of measured microhardness near the mid-radius of the HPT disks is presented in Figure 7(a). The mean microhardness increases significantly from the initial state of ~198 Hv to ~ 390 Hv after 0.5 turn. This strengthening is continuous with further torsional straining to reach a value of ~475 Hv after 20 turns. A similar microhardness evolution was reported in an Fe-50%Ni (at. %) alloy processed by HPT at room temperature for up to 10 turns [35] and in an Invar^{TM} (Fe36%Ni) alloy [36]. The hardening is often ascribed to the increase in dislocation density and concomitant grain refinement [37–39].

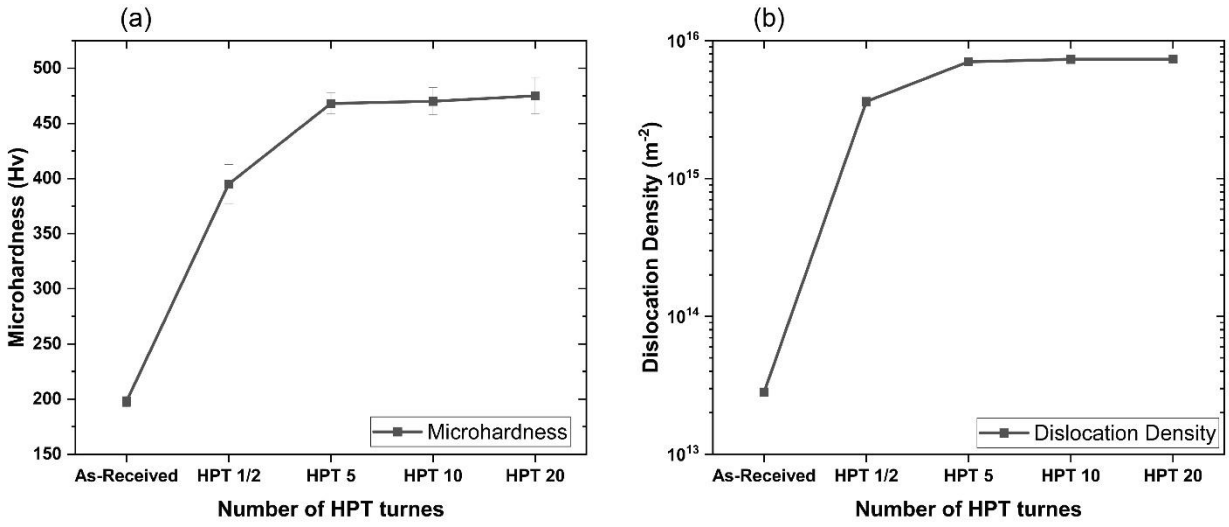

Figure 7: Evolution of a) the hardness and b) the dislocation density (ρ) using the KAM method at mid-radius of the Permimphy^{TM} alloy after HPT processing and annealing.

The assessed dislocation density (ρ) using the KAM method is shown in Figure 7(b). Thus, ρ significantly increased after 1/2 HPT turn to reach 3.62×10^{15} m^{-2} compared to 2.82×10^{13} m^{-2} for the as-received sample (not shown in the plot). This large difference is mainly caused by the formation of dislocations and their accumulation as shown in Figure 7(b). Furthermore, the dislocation density appears to level off around 7.3×10^{15} m^{-2} after 10 HPT turns. This is mainly attributed to the effect of the steady-state generation of the dislocations and their annihilation. Furthermore, this steady-state dislocation generation and annihilation is synergistically accompanied by a stabilization of the grain size as shown in Figure 3.

Figure 8 provides a more detailed understanding of the evolution of dislocation density during the HPT deformation. After 1/2 turns of HPT, a considerable number of dislocations is generated since various slip systems are activated. This activation induces local rotations of the crystal and generates misorientations with neighboring regions. Consequently, geometrically necessary boundaries (GNBs) are formed as observed in the KAM. As HPT deformation continues,

the initial grains undergo subdivision by accumulating GNBs, leading to the formation of finer nanoscale subdivided structures characterized by HAGBs)

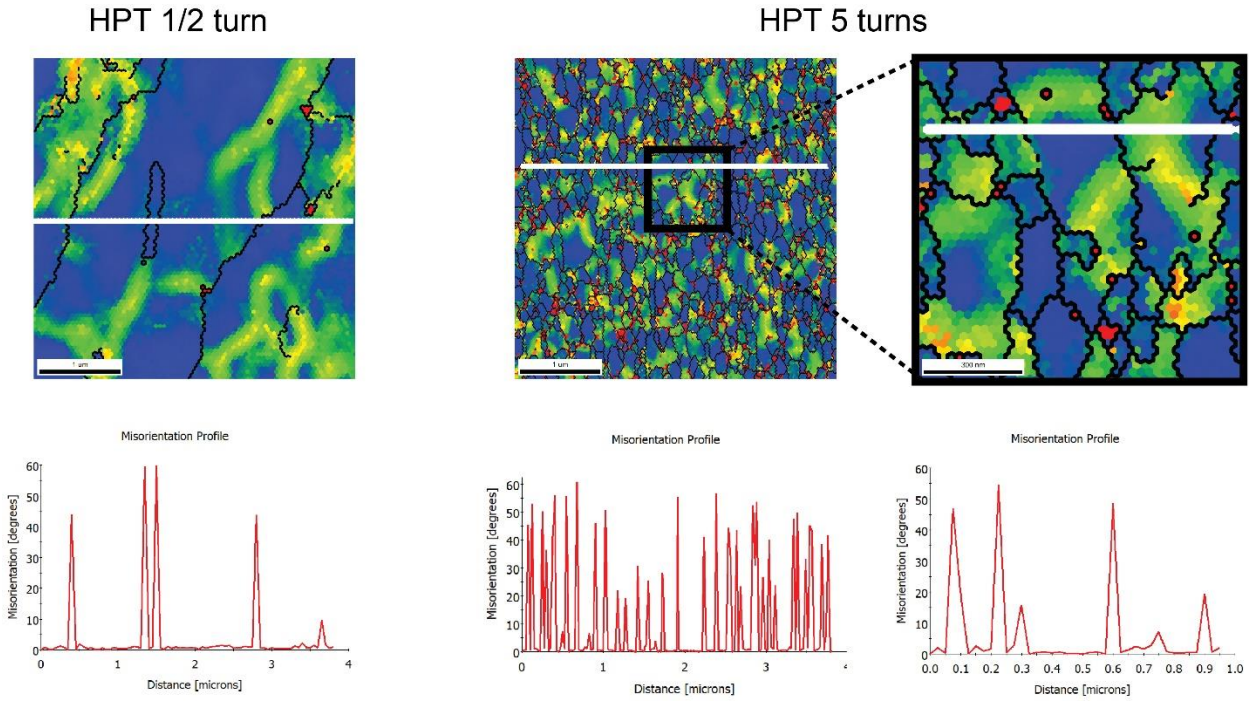

Figure 8 : Higher magnification KAM maps after 1/2 and 10 HPT turns.

It is important to note that these new grains contain a substantial number of geometrically necessary dislocations (GNDs). This observation explains the higher values of dislocation density observed in the more highly deformed states, such as at 5 turns or more, compared to the dislocation density after 1/2 turn. This difference can be clearly observed by comparing the deformed zones (green/orange) in the same area size for the two deformation states of 1/2 and 5 turns in Figure 8.

3.4 Evolution of the magnetic properties after SPD

Figure 9 presents the hysteresis curves of magnetization M as a function of applied field H for the Permimphy^{TM} alloy processed by HPT deformation up to 20 turns. The saturation magnetization M_s and the coercive field H_c were deduced from the curves. It is readily apparent

that the curves are very close and hard to distinguish. This is a well-known characteristic feature of soft magnetic materials. A close inspection of Figure 9(b) shows that following 1/2 HPT turn there was a noticeable expansion in the loops when compared to the initial state. This enlargement is attributed to the introduction of dislocations into the microstructure which impedes both domain wall motion and domain rotation [40]. However, it may also be associated with grain refinement, particularly given that the materials in question are polycrystalline and initially possess relatively large grains [12].

After undergoing 10 HPT turns, there was a reduction in the loop thickness. As illustrated in Figure 2, the average grain size at this stage was approximately 200 nm. Given the consistently high dislocation density, it is readily deduced that this reduction in hysteresis loop size was associated with the microstructural refinement. Furthermore, following 20 HPT turns, the loop thickness, or coercivity, increased again, but not significantly. In this case, it is probably due to the interplay of two opposed effects: the dislocation density which has an adverse impact on magnetic softness and the microstructure refinement which exerts a positive influence on coercivity. As depicted in Figure 2, the grain size difference between the samples after 10 and 20 HPT turns was minimal at approximately ~200 nm. Therefore, the dominant effect was attributed to the dislocation density.

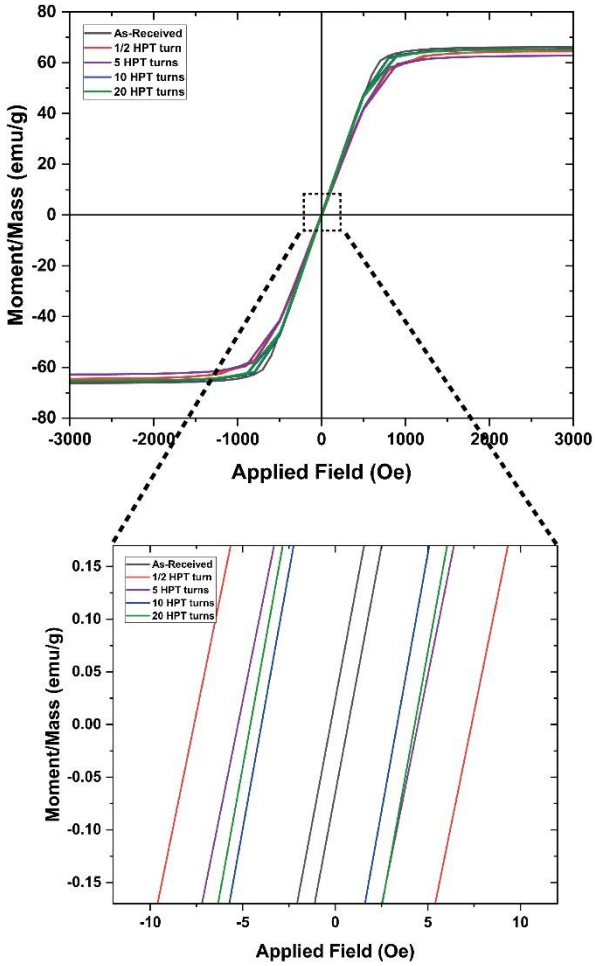

Figure 9 : Hysteresis loops of the as-received and HPT-deformed Permimphy alloy.

A ferromagnetic behavior is indicated by a continuous increase of the magnetization under small fields. At very high magnetic fields the magnetization of the samples reaches a saturation level. The grain size is also known to influence the coercivity (*H*c). The relationship between coercivity and grain size and with the inverse of the hardness for the Permimphy^{TM} after SPD processing can now be highlighted as shown in Figure 10. To obtain a comprehensive understanding of the relationship between coercivity (*H*c), grain size (*d*) and Vickers hardness (*Hv*), additional findings from an ongoing project conducted by the same authors are included in the Figures 10(a) and (b). These results showcase samples of the Permimphy^{TM} alloy that underwent deformation using the accumulative roll bonding (ARB) and constraint groove pressing

(CGP) methods of SPD processing although in practice HPT was the best technique for achieving grain refinement. Furthermore, the plot is augmented with datum points from three additional samples of the Invar alloy that underwent HPT deformation and serve as a comparative reference.

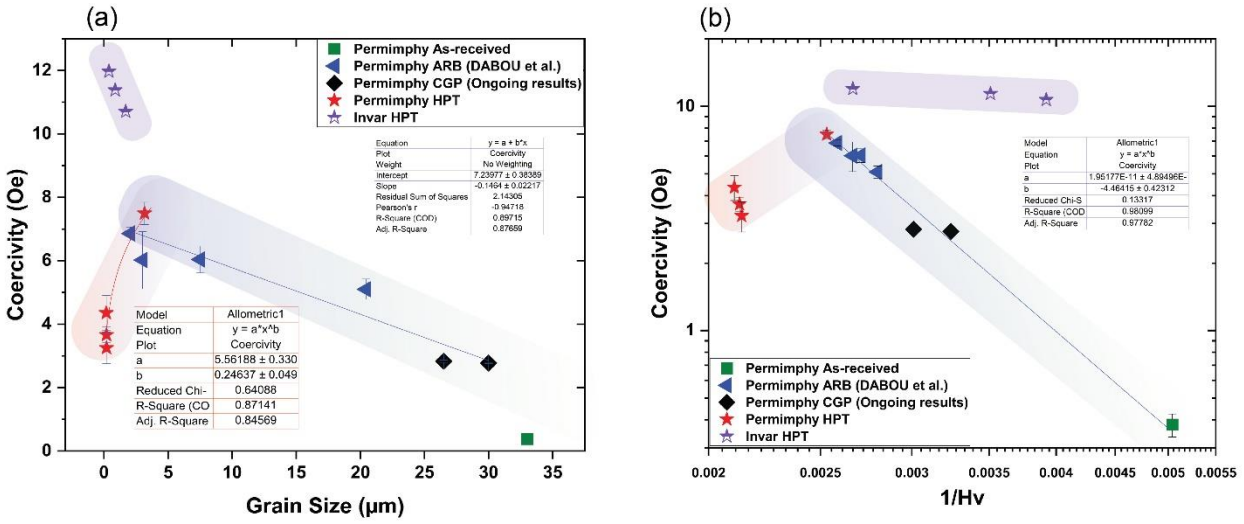

Figure 10 : Evolution of the coercivity with (a): the mean grains size, (b): the inverse of hardness for the Permimphy/Invar after SPD.

As shown in a study of soft magnetic alloys [9-11], the effect of grain size on coercivity falls into two distinct regimes. When the grain size d exceeds the ferromagnetic exchange length, Hc of a magnetic material is known to be proportional to d^{-1}, whereas Hc becomes proportional to d^6 when d is less than the ferromagnetic exchange length. There is also other research investigating the evolution of magnetic properties after SPD processing [34-39]. Indeed, there is a study of the microstructure and magnetic properties in nanostructured Fe and Fe-Based intermetallic produced by HPT [43]. The minimum grain sizes obtained by HPT deformation were 265 nm for pure iron, 152 nm for FeCo and 207 nm for FeNi3, respectively. It seems conclusive that the minimum grain size attained by HPT deformation in pure iron, FeCo and FeNi3 can never reach a value below 100 nm and thus the coercivity follows the d^{-1} law [10]. There is a report that lattice defects play a

dominant role in magnetic properties for coarse grain material after ECAP of the 49Fe-49Co-2V alloy [47].

In the present study, after 1/2 HPT turn the grain size was reduced from 30 to 3 μm (~ 90%) and *H*c increased from 0.38 to 7.59 Oe (x15). This is expected since the movement of magnetic domain walls is hindered by grain boundaries and dislocations. It is clear that an increase in d (when $d > 3\mu m$) leads to a decrease in *H*c Figure 10(a) is consistent with the earlier observations on traditional polycrystalline materials [10]. Surprisingly, for grain sizes below 3 μm *H*c decreases despite an increase in both dislocation density and microhardness. This phenomenon is a consequence of the grains becoming smaller than the ferromagnetic exchange length of the Permimphy alloy which is around 1 to 3 μm [14]. The behavior of the Permimphy after HPT differs from that of the Fe36Ni (Invar) alloy as observed in these studies where *H*c increases with decreasing grain size (as represented by the purple points in Figure 10(a)). This finding is consistent with the fact that the grain size of this deformed Invar is larger than its magnetic exchange length which is approximately 0.1 to 0.2 μm [14].

These observations confirm the unique magnetic properties of the Permimphy in this study. However, the decrease in *H*c does not follow the d^6 behavior which may be due to the high dislocation density in the samples used in this study whereas earlier research dealt only with partially amorphous and nanocrystalline materials that were annealed to minimize ρ [10, 11]. At this stage, it is reasonable to assume that the grain refinement plays a dominant role compared with the dislocation density.

For the evolution of *H*c as a function of the microhardness in Figure 10 (b)), it was found that for d >3 μm then

$$Hc = 2 * Hv^{4.5} 10^{-11}\, Oe \quad \ldots\ldots\ldots\ldots\ldots \quad \text{Equation 2}$$

This means that, in the deformed polycrystalline materials, *H*c can be predicted from a simple microhardness test using equation 2. In practice, *H*c is expected to depend on microhardness which increases with the presence of all types of defects such as grain boundaries, voids, dislocations and dislocation cells. These features serve as pinning sites for the magnetic domain walls which in turn increases the coercivity. There is a report on the effect of the dislocation pattern on the magnetic domain structure of pure polycrystalline Ni and it was found that the presence of deformation structure in the ferromagnetic metals can impede any magnetic domain motion and thereby affect the magnetic properties [47]. Also, an investigation of the influence of dislocations on domain walls by using magneto-mechanical hysteresis modeling revealed that the dislocation pinning effect is proportional to the n^{-th} power of the dislocation density which is the underlying mechanism for increasing the coercivity [48] .

The results presented in this study show that the coercivity decreases with decreasing grain size, however HPT under the present conditions produces a steady state of grain refinement even with further HPT deformation. Another possibility for further reducing the coercivity is to perform an annealing after HPT deformation in order to decrease and minimize the dislocation density without any significant further increase of the grain size. Both considerable hardness (owing to the UFG microstructure) and a very small coercivity would be expected after HPT deformation and adequate annealing. In an accompanying investigation, Dabou et al, [49] have processed the same alloy via ARB up to 5 cycles. This resulted in a grain size reduction down to 2.2 µm, a hardness of 375 Hv, a dislocation density of 1.9×10^{15} m^{-2} and a coercivity of 6.8 Oe. After annealing at 650°C for one hour, the alloy experienced recrystallization and grain growth, resulting in a mean grain size of 4.5 µm, a hardness of 250 Hv, a dislocation density of 3.5×10^{14} m^{-2} and a notable

increase in coercivity to 0.2 Oe. In the current study, processing the same alloy to 20 HPT turns resulted in a much considerable grain refinement (about 200 nm), higher hardness (about 475 Hv), but with a high coercivity of about 6.8 Oe, likely due to the elevated dislocation density, as previously discussed. According to the author's, the most effective post-HPT processing annealing conditions are expected to be 600°C to 650°C under a controlled atmosphere for less than an hour, followed by quenching. This process is expected to yield a coercivity below 0.1 Oe, a grain size less than 1 μm, and a substantial hardness exceeding 400 Hv.

In addition, ongoing research has focused on studying the super-magnetism phenomena of the alloy at very low temperatures (from 30 up to 300 K). There is a report of the existence of super-paramagnetic (SPM) behavior of nanocrystalline cobalt-iron-pyrite samples with antiferromagnetic clusters suppressing magnetic dipolar interactions [50]. The reported crystalline size was about 15 to 7 nm. In the case of the Permimphy alloy, since its exchange length is about 1 to 3 μm, it is challenging to seek a possible supermagnetic behaviour at the submicron level but this is the target of an ongoing research activity.

4. Summary and conclusions

The evolution of microstructure, hardness and the dislocation density of the Permimphy alloy, as well its magnetic characteristic after HPT deformation, was studied in this research in order to reveal a possible correlation between the grain size (d) and the coercivity (H). The results led to the following conclusions.

1) The grain size of the Permimphy alloy was remarkably refined after severe plastic deformation particularly after HPT deformation. The grain size distribution of the HPT-

deformed alloy after 1/2 turn was inhomogeneous whereas after 5 or more turns it was homogeneous with an average grain size of about 190 nm.

2) The mechanical properties of the alloy were significantly improved after 5 HPT turns. The microhardness was 470 Hv (+140% compared to the as-received state) due to the grain refinement and dislocation density.
3) For grain sizes greater than 3 µm, an increase in d leads to a decrease in *H*c, which is consistent with earlier observations on traditional polycrystalline materials. However, for grain sizes below 3 µm, *H*c decreases despite an increase in the dislocation density and microhardness. This effect arises because the grains become smaller than the ferromagnetic exchange length of Permimphy (1-3 µm). In the case of Invar alloy, *H*c increases with decreasing grain size since the grain size is larger than its magnetic exchange length (100-200 nm).
4) The use of SPD processing is an efficient approach for creating materials with robust magnetic and mechanical characteristics. However, for soft magnetic materials it appears that a heat treatment may be required after HPT processing to restore the magnetic softness of the material. It is concluded that using an adequate annealing to remove the dislocation density without increasing the grain size will lead to significant results for both the mechanical and magnetic behaviour.

Acknowledgements

Two of the authors were supported by the European Research Council under Grant Agreement No. 267464-SPDMETALS (YH and TGL).

Data availability

Some data included in this work are available upon request by contact with the corresponding author.

Contributions

Oussama Dabou (M.Sc.): Investigation, Validation, Writing, Visualization.

Thierry Baudin (Dr.): Methodology, Review and Editing, Visualization.

François Brisset (Dr.) : Methodology, Investigation.

Thierry Waeckerlé (Dr.) : Methodology, Review

Yanick Ateba Betanda (Dr.) : Methodology, Review

Yi Huang (Prof.) : Methodology, Review and Editing.

Anne-Laure Helbert (Prof.): Conceptualization, Writing, Original draft, Review and Editing, Visualization and Supervision.

Djamel Bradai (Prof.): Conceptualization, Writing, Original draft, Review and Editing, Visualization and Supervision.

Terence G. Langdon (Prof.): Review and Editing.

Conflict of interest

The authors declare no competing financial or personal interests concerning the work reported in this manuscript to the best of their knowledge.

Ethical approval

Not applicable.

Supplementary information

Not applicable.

Bibliography

1. Czichos H, Saito T, Smith LR (2006) Springer handbook of materials measurement methods. Springer, Germany

2. Ouyang G, Chen X, Liang Y, et al (2019) Review of Fe-6.5 wt%Si high silicon steel—A promising soft magnetic material for sub-kHz application. J Magn Magn Mater 481:234–250. https://doi.org/10.1016/j.jmmm.2019.02.089

3. Gutfleisch O, Willard MA, Brück E, et al (2011) Magnetic Materials and Devices for the 21st Century: Stronger, Lighter, and More Energy Efficient. Adv Mater 23:821–842. https://doi.org/10.1002/adma.201002180

4. Waeckerlé T, Demier A, Godard F, Fraisse H (2020) Evolution and recent developments of 80%Ni permalloys. J Magn Magn Mater 505:166635. https://doi.org/10.1016/j.jmmm.2020.166635

5. PERMIMPHY is a 80% Nickel soft magnetic alloy. In: aperam. https://www.aperam.com/product/permimphy-80-nickel/. Accessed 3 Apr 2023

6. Han L, Maccari F, Souza Filho IR, et al (2022) A mechanically strong and ductile soft magnet with extremely low coercivity. Nature 608:310–316. https://doi.org/10.1038/s41586-022-04935-3

7. Nabi B, Helbert A-L, Brisset F, et al (2013) Effect of recrystallization and degree of order on the magnetic and mechanical properties of soft magnetic FeCo–2V alloy. Mater Sci Eng A 578:215–221. https://doi.org/10.1016/j.msea.2013.04.066

8. Nabi B, Helbert A-L, Brisset F, et al (2014) Effect of long range order on mechanical properties of partially recrystallized Fe49Co–2V alloy. Mater Sci Eng A 592:70–76. https://doi.org/10.1016/j.msea.2013.10.093

9. Herzer G (1989) Grain structure and magnetism of nanocrystalline ferromagnets. IEEE Trans Magn 25:3327–3329. https://doi.org/10.1109/20.42292

10. Herzer G (1990) Grain size dependence of coercivity and permeability in nanocrystalline ferromagnets. IEEE Trans Magn 26:1397–1402. https://doi.org/10.1109/20.104389

11. Herzer G (1997) Chapter 3 Nanocrystalline soft magnetic alloys. In: Handbook of Magnetic Materials. Elsevier, pp 415–462

12. Herzer G (2013) Modern soft magnets: Amorphous and nanocrystalline materials. Acta Mater 61:718–734. https://doi.org/10.1016/j.actamat.2012.10.040

13. Suzuki K, Ito N, Garitaonandia JS, et al (2008) Local random magnetocrystalline and macroscopic induced anisotropies in magnetic nanostructures. J Non-Cryst Solids 354:5089–5092. https://doi.org/10.1016/j.jnoncrysol.2008.06.118

14. Pfeifer F, Radeloff C (1980) Soft magnetic Ni-Fe and Co-Fe alloys - some physical and metallurgical aspects. J Magn Magn Mater 19:190–207. https://doi.org/10.1016/0304-8853(80)90592-2

15. Zhilyaev AP, Langdon TG (2008) Using high-pressure torsion for metal processing: Fundamentals and applications. Prog Mater Sci 53:893–979. https://doi.org/10.1016/j.pmatsci.2008.03.002

16. Saito Y, Utsunomiya H, Tsuji N, Sakai T (1999) Novel ultra-high straining process for bulk materials—development of the accumulative roll-bonding (ARB) process. Acta Mater 47:579–583. https://doi.org/10.1016/S1359-6454(98)00365-6

17. Valiev RZ, Langdon TG (2006) Principles of equal-channel angular pressing as a processing tool for grain refinement. Prog Mater Sci 51:881–981. https://doi.org/10.1016/j.pmatsci.2006.02.003

18. Zhilyaev AP, Kim B-K, Nurislamova GV, et al (2002) Orientation imaging microscopy of ultrafine-grained nickel. Scr Mater 46:575–580. https://doi.org/10.1016/S1359-6462(02)00018-0

19. Zhilyaev AP, Nurislamova GV, Kim B-K, et al (2003) Experimental parameters influencing grain refinement and microstructural evolution during high-pressure torsion. Acta Mater 51:753–765. https://doi.org/10.1016/S1359-6454(02)00466-4

20. Azzeddine H, Bradai D, Baudin T, Langdon TG (2022) Texture evolution in high-pressure torsion processing. Prog Mater Sci 125:100886. https://doi.org/10.1016/j.pmatsci.2021.100886

21. Wongsa-Ngam J, Kawasaki M, Langdon TG (2013) A comparison of microstructures and mechanical properties in a Cu–Zr alloy processed using different SPD techniques. J Mater Sci 48:4653–4660. https://doi.org/10.1007/s10853-012-7072-0

22. Figueiredo RB, Pereira PHR, Aguilar MTP, et al (2012) Using finite element modeling to examine the temperature distribution in quasi-constrained high-pressure torsion. Acta Mater 60:3190–3198. https://doi.org/10.1016/j.actamat.2012.02.027

23. Ateba Betanda Y, Helbert A-L, Brisset F, et al (2014) Measurement of stored energy in Fe–48%Ni alloys strongly cold-rolled using three approaches: Neutron diffraction, Dillamore and KAM approaches. Mater Sci Eng A 614:193–198. https://doi.org/10.1016/j.msea.2014.07.037

24. Azzeddine H, Tirsatine K, Baudin T, et al (2017) On the stored energy evolution after accumulative roll-bonding of invar alloy. Mater Chem Phys 201:408–415. https://doi.org/10.1016/j.matchemphys.2017.08.063

25. Bate PS, Knutsen RD, Brough I, Humphreys FJ (2005) The characterization of low-angle boundaries by EBSD. J Microsc 220:36–46. https://doi.org/10.1111/j.1365-2818.2005.01513.x

26. Pippan R, Scheriau S, Taylor A, et al (2010) Saturation of Fragmentation During Severe Plastic Deformation. Annu Rev Mater Res 40:319–343. https://doi.org/10.1146/annurev-matsci-070909-104445

27. Rathmayr GB, Pippan R (2011) Influence of impurities and deformation temperature on the saturation microstructure and ductility of HPT-deformed nickel. Acta Mater 59:7228–7240

28. Renk O, Pippan R (2019) Saturation of grain refinement during severe plastic deformation of single phase materials: reconsiderations, current status and open questions. Mater Trans 60:1270–1282

29. Tsuji N, Kamikawa N, Li BL (2007) Grain size saturation during severe plastic deformation. In: Materials science forum. Trans Tech Publ, pp 2837–2842

30. Yu T, Hansen N, Huang X (2011) Recovery by triple junction motion in aluminium deformed to ultrahigh strains. Proc R Soc Math Phys Eng Sci 467:3039–3065. https://doi.org/10.1098/rspa.2011.0097

31. Yu T, Hansen N, Huang X, Godfrey A (2014) Observation of a new mechanism balancing hardening and softening in metals. Mater Res Lett 2:160–165

32. Tsuji N (2008) Formation mechanisms of ultrafine grained structures in severe plastic deformation of metallic materials. J Iron Steel Inst Jpn 94:582–589

33. Humphreys FJ, Hatherly M (2012) Recrystallization and related annealing phenomena. Elsevier

34. Kawasaki M (2014) Different models of hardness evolution in ultrafine-grained materials processed by high-pressure torsion. J Mater Sci 49:18–34. https://doi.org/10.1007/s10853-013-7687-9

35. Lee SW, Horita Z (2010) Annealing Behavior of FeNi Alloy Processed by High-Pressure Torsion. Mater Sci Forum 667–669:313–318. https://doi.org/10.4028/www.scientific.net/MSF.667-669.313

36. Tirsatine K, Azzeddine H, Huang Y, et al (2018) An EBSD analysis of Fe-36%Ni alloy processed by HPT at ambient and a warm temperature. J Alloys Compd 753:46–53. https://doi.org/10.1016/j.jallcom.2018.04.194

37. Tirsatine K, Azzeddine H, Baudin T, et al (2014) Texture and microstructure evolution of Fe–Ni alloy after accumulative roll bonding. J Alloys Compd 610:352–360. https://doi.org/10.1016/j.jallcom.2014.04.173

38. Bonnot E, Helbert A-L, Brisset F, Baudin T (2013) Microstructure and texture evolution during the ultra grain refinement of the Armco iron deformed by accumulative roll bonding (ARB). Mater Sci Eng A 561:60–66. https://doi.org/10.1016/j.msea.2012.11.017

39. Boudekhani S, Azzeddine H, Tirsatine K, et al (2018) Microstructure, Texture, and Mechanical Properties of Ni-W Alloy After Accumulative Roll Bonding. J Mater Eng Perform 27:5561–5570. https://doi.org/10.1007/s11665-018-3628-8

40. Cullity BD, Graham CD (2011) Introduction to Magnetic Materials. John Wiley & Sons

41. Glezer AM, Muradimova LF, Shirshikov SO, et al (2019) Effect of Large Plastic Deformations in a Bridgman Chamber on the Structure and Properties of FeCo–V Alloys. Bull Russ Acad Sci Phys 83:1250–1260. https://doi.org/10.3103/S1062873819100083

42. Glezer AM, Muradimova LF, Borisova PA, et al (2021) EXAFS-spectroscopy and thermal neutron diffraction study of the effect of deformation by high pressure torsion on the atomic ordering and magnetic properties of the FeCo alloy. J Alloys Compd 866:159021. https://doi.org/10.1016/j.jallcom.2021.159021

43. Hosokawa A, Ohtsuka H, Li T, et al (2014) Micostructure and Magnetic Properties in Nanostructured Fe and Fe-Based Intermetallics Produced by High-Pressure Torsion. Mater Trans 55:1286–1291. https://doi.org/10.2320/matertrans.M2014119

44. Paul A, Liu X, Kawasaki M, Liss K-D (2023) Inverted magnetic response in severe plastically deformed nanostructured high-entropy alloy. Appl Phys Lett 122:052402. https://doi.org/10.1063/5.0138040

45. Wang Y, Xu J, Liu Y, Liu Z (2022) Microstructure evolution, magnetic properties and frequency characteristics of Si-rich FeSiBCuNb soft magnetic alloy induced by annealing treatment. Mater Charact 187:111830. https://doi.org/10.1016/j.matchar.2022.111830

46. Susan DF, Kustas AB, Kellogg RA, et al (2021) The Effects of Annealing After Equal Channel Angular Extrusion (ECAE) on Mechanical and Magnetic Properties of 49Fe-49Co-2V Alloy. Metall Mater Trans A 52:4090–4099. https://doi.org/10.1007/s11661-021-06366-7

47. Xiang Z, Sun Q, Wang S (2022) Effect of dislocation pattern on the magnetic domain structure of pure polycrystalline Ni. J Mater Res Technol 17:1896–1900. https://doi.org/10.1016/j.jmrt.2022.01.107

48. Lo CCH, Kinser E, Jiles DC (2003) Modeling the interrelating effects of plastic deformation and stress on magnetic properties of materials. J Appl Phys 93:6626–6628. https://doi.org/10.1063/1.1557356

49. Dabou O, Bensouilah A, Baudin T, et al (2023) Evolution of the texture, microstructure, and magnetic properties of a Permimphy alloy after accumulative roll bonding and aging. J Mater Sci. https://doi.org/10.1007/s10853-023-08994-3

50. Gabold H, Luan Z, Paul N, et al (2018) Structural and magnetic properties of cobalt iron disulfide (CoxFe1−xS2) nanocrystals. Sci Rep 8:4835. https://doi.org/10.1038/s41598-018-22996-1